REPORT DOCUMENTATION PAGE

Form Approved
OMB No. 074-0188

Public reporting burden for this collection of information is estimated to average 1 hour per response, including the time for reviewing instructions, searching existing data sources, gathering and maintaining the data needed, and completing and reviewing this collection of information. Send comments regarding this burden estimate or any other aspect of this collection of information, including suggestions for reducing this burden to Washington Headquarters Services, Directorate for Information Operations and Reports, 1215 Jefferson Davis Highway, Suite 1204, Arlington, VA 22202-4302, and to the Office of Management and Budget, Paperwork Reduction Project (0704-0188), Washington, DC 20503

1. AGENCY USE ONLY (Leave blank)	2. REPORT DATE Feb. 1996	3. REPORT TYPE AND DATES COVERED Proceedings, February 1996.

4. TITLE AND SUBTITLE	5. FUNDING NUMBERS
Numerical Model of a Photolytic Reactor for VOC Destruction	N/A

6. AUTHOR(S)
M.R. Mallery & R.J. Heinsohn

7. PERFORMING ORGANIZATION NAME(S) AND ADDRESS(ES)	8. PERFORMING ORGANIZATION REPORT NUMBER
140 Reber Building Pennsylvania State University University Park, PA 16802	ES96-47

19980709 128

9. SPONSORING / MONITORING AGENCY NAME(S) AND ADDRESS(ES)	10. SPONSORING / MONITORING AGENCY REPORT NUMBER
SERDP 901 North Stuart St. Suite 303 Arlington, VA 22203	N/A

11. SUPPLEMENTARY NOTES

Proceedings of the Air & Waste Management Association Conference on Emerging Solutions to VOC and Air Toxics Control, Clearwater, FL, February 1996. No copyright is asserted in the United States under Title 17, U.S. code. The U.S. Government has a royalty-free license to exercise all rights under the copyright claimed herein for Government purposes. All other rights are reserved by the copyright owner.

12a. DISTRIBUTION / AVAILABILITY STATEMENT	12b. DISTRIBUTION CODE A
Approved for public release: distribution is unlimited	

13. ABSTRACT (Maximum 200 Words)

A computational fluid dynamics (CFD) model has been developed which describes the interaction between the fluid dynamics of a volatile organic compound (VOC) laden gas stream and the photochemical processes occurring within a photolytic reactor. The VOCs chosen for study are formaldehyde and methanol, and it is the goal of this paper to describe the mechanisms which most directly influence the destruction of formaldehyde in the reactor.

Modeling studies show how formaldehyde destruction in the reactor is influenced by the distribution of ultraviolet energy in the reactor, the gas stream residence time and the inlet ozone dosage to the reactor. It was found that increasing the inlet ozone dose, increasing the gas stream residence time and increasing the light intensity all produced higher rates of formaldehyde destruction.

14. SUBJECT TERMS	15. NUMBER OF PAGES
Photolytic reactor, VOCs, Ozone, Ultraviolet energy, Formaldehyde, SERDP	12
	16. PRICE CODE N/A

17. SECURITY CLASSIFICATION OF REPORT	18. SECURITY CLASSIFICATION OF THIS PAGE	19. SECURITY CLASSIFICATION OF ABSTRACT	20. LIMITATION OF ABSTRACT
unclass.	unclass.	unclass.	UL

NSN 7540-01-280-5500

Standard Form 298 (Rev. 2-89)
Prescribed by ANSI Std. Z39-18
298-102

DTIC QUALITY INSPECTED 1

Numerical Model of a Photolytic Reactor for VOC Destruction

Meryl Reis Mallery and Robert Jennings Heinsohn
140 Reber Building
Pennsylvania State University
University Park, PA 16802

ABSTRACT

A computational fluid dynamics (CFD) model has been developed which describes the interaction between the fluid dynamics of a volatile organic compound (VOC) laden gas stream and the photochemical and chemical processes occurring within a photolytic reactor. The VOCs chosen for study are formaldehyde and methanol, and it is the goal of this paper to describe the mechanisms (fluid dynamic, chemical or photochemical) which most directly influence the destruction of formaldehyde in the reactor.

Modeling studies show how formaldehyde destruction in the reactor is influenced by the distribution of ultraviolet energy in the reactor, the gas stream residence time and the inlet ozone dosage to the reactor. It was found that increasing the inlet ozone dose, increasing the gas stream residence time and increasing the light intensity all produced higher rates of formaldehyde destruction.

INTRODUCTION

Passage of the Clean Air Act Amendments by Congress in 1990 is placing more stringent control on VOC emissions. These emerging regulations are forcing industries to reduce VOC emissions through new manufacturing techniques or through the use of air pollution control equipment. An emerging air pollution control technology is the use of ultraviolet (UV) photochemical and radical oxidation to destroy pollutant VOCs in process gas streams. A commercial system based in part on this technology has been developed and a pilot scale version has been installed at the Applied Research Laboratory (ARL) at The Pennsylvania State University. Research is currently being performed with the pilot scale system to determine the system's effectiveness in removing different classes of VOCs and to recommend design improvements that enhance VOC destruction throughout the system. A numerical model of the photolytic reactor in the pilot scale system has been developed in support of this research effort.

The numerical model is used to predict the gas velocities and chemical species concentrations as a function of spatial location within the reactor under steady state conditions. Formaldehyde (HCHO) in moist air with trace amounts of ozone is used to evaluate the reactor performance.

PHYSICAL SYSTEM DESCRIPTION

The photolytic reactor design modeled in this study is provided in Figure 1. The reactor is a rectangular duct containing two cylindrical lamps in series which emit electromagnetic radiation in the ultraviolet light spectrum. An air stream containing formaldehyde, methanol, ozone and water vapor enters the reactor from the left and passes perpendicular to the lamp axes. As the VOC laden gas stream passes over the lamps, O_3, H_2O_2 and HCHO absorb electromagnetic radiation which leads to the dissociation of these species.

The reactor is 0.19 meters (7.5 inches) tall and 0.54 meters (21 inches) long. Two TQ 718 (700 W) medium-pressure mercury arc lamps manufactured by Hereaus Amersil in Germany provide energy

over the wavelength range 238 to 579 nm (ultraviolet). The bulb diameters are 0.0635 meters (2.5 inches) and are placed in the center of the reactor.
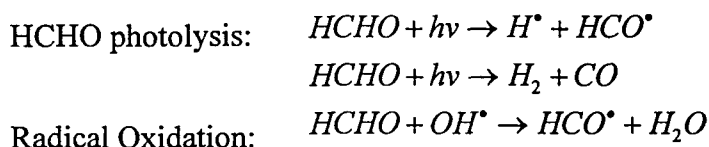
MODEL DESCRIPTION

The mathematical model of the reactor was constructed using Harwell (CFDS)-FLOW3D, which is a Computational Fluid Dynamics (CFD) package developed by Harwell Laboratory in the United Kingdom. The photolytic reactor model consists of three components:

1)   a description of the light intensity distribution in the reactor
2)   a description of the reaction kinetics for HCHO destruction in air in the presence of UV light
3)   a description of the velocity field through the reactor.

A two-dimensional model of the reactor was developed based on the design configuration provided in Figure 1. Steady-state predictions of air stream velocity and chemical species concentrations as a function of spatial location within the reactor are generated to evaluate the efficiency of the reactor in removing HCHO.

Light Intensity Model

The strength and distribution of the ultraviolet energy source at given wavelengths plays a crucial role in the destruction of HCHO in the photolytic reactor. HCHO is destroyed in the reactor through two primary routes (Calvert et al., 1966):

HCHO photolysis: $HCHO + hv \rightarrow H^{\bullet} + HCO^{\bullet}$

$HCHO + hv \rightarrow H_2 + CO$

Radical Oxidation: $HCHO + OH^{\bullet} \rightarrow HCO^{\bullet} + H_2O$

The radical oxidation process is dependent on the production of $OH^{\bullet}$ radicals from the photolysis of O_3 and to a minor extent on the photolysis of H_2O_2. Two $OH^{\bullet}$ radicals are produced from the reaction of (O^1D) radicals (produced from O_3 photolysis) with water vapor (Demore et al., 1992). The photolytic rate constants for these processes (HCHO, O_3 and H_2O_2 photolysis) are dependent on the strength and distribution of electromagnetic radiation in the reactor. Assuming that the TQ 718 lamps emit radiation solely in the radial direction, the integrated form of the Beer-Lambert Law is applied to calculate the photolytic rate constants at ambient conditions. This is illustrated with equation (1) which predicts the light intensity distribution in the reactor. It is assumed with the use of equation (1) that HCHO and O_3 are the only chemical species which contribute significantly to light attenuation in the reactor. This assumption is based on a review of the absorption cross-sections multiplied by the species concentrations analyzed in the model (Mallery, 1995).

$$I_r = \frac{r_o I_{ro}}{r} e^{-(r-r_o)\sum [C]\sigma} \tag{1}$$

The photolytic rate constants for HCHO, O_3 and H_2O_2 are then calculated with equation (2) which takes into account the radial variation in the intensity distribution derived in equation (1).

$$k = \frac{r_o}{r} \sum_{\lambda_1}^{\lambda n} \sigma(\lambda,T)\phi(\lambda,T) e^{-(r-r_o)\sum[C]} J(\lambda) \tag{2}$$

where $\phi(\lambda, T)$ is the quantum yield of the reaction

$\sigma(\lambda, T)$ is the absorption cross-section of a given molecule and

$J(\lambda)$ is the actinic flux emitted by the light source

The quantum yield accounts for the fact that not all of the light energy absorbed by a molecule results in dissociation of the molecule, and the absorption cross-section is a measure of the probability that the interaction between the electromagnetic wave and the molecular cross-section will lead to absorption of a quantum of light energy. As can be seen by equation (2), the photolytic rate constants are calculated by summing over discrete wavelengths. Twelve wavelengths were analyzed that ranged between 248 and 366 nm. Equation (2) also illustrates that the photolytic rate constants vary inversely with radial distance from the bulb surface.

Chemical Kinetics Model

Twenty-three chemical reactions involving 14 chemical species are analyzed in the model. This is a reduced chemical kinetic model for the oxidation of HCHO in the presence of ultraviolet light and O_3 based on a more complex system consisting of 56 chemical reactions for 21 chemical species that were compiled from the literature (Schmelzle, 1994 and Albano, 1994). A reduced chemical equation set is essential for use in flow field modeling to reduce computational time and cost. The validity of the reduced chemical kinetic model was verified by comparing predictions for the two chemical kinetic models under well-mixed reactor conditions. It was found that the reduced chemical kinetic model was valid for the residence times analyzed in the reactor under study.

The kinetic mechanisms are incorporated into the flow field model by introducing the species mass conservation equation for each of the following chemical species: HCHO, CH_3OH, $OH^\bullet$, $H^\bullet$, $HO_2^\bullet$, $O(^3P)$, $O(^1D)$, H_2O_2, O_3, HCO and CO. Water vapor, O_2 and N_2 species are also included in the model but it is assumed that their concentrations remained fixed throughout the calculation process. This assumption is valid since the species have a large concentration within the reactor and have slow rates of removal.

The kinetic mechanisms which lead to generation or removal of a given species are incorporated as source/sink terms, symbolized by S, in the species mass conservation equation given below:

$$\rho \bar{u}_j \frac{\partial C}{\partial x_j} - \frac{\partial}{\partial x_j}\left(\left(\frac{\mu T}{\sigma_s} + \rho D\right)\frac{\partial C}{\partial x_j}\right) = S \tag{3}$$

$$S = S_p C + S_u \tag{4}$$

This equation includes advection, diffusion and chemical transformation for a given chemical species. To account for the chemical reaction kinetics in each scalar equation, the source term is linearized into two components: S_p and S_u. S_p includes all source terms which contain the dependent variable and act as a sink for that variable. S_u contains all other source terms including those terms which act as a source for the dependent variable. Table 1 provides the chemical reactions included in the kinetic model along with their rate constants.

Flow Field Model

Time averaged velocity distributions are calculated in the reactor using the Reynolds Averaged Navier-Stokes (RANS) form of the momentum equation and the mass conservation equation. A two-

equation k-ε turbulence model with incompressible Newtonian flow is also assumed with this model. The photolytic reactor geometry provided in Figure 1 was modeled with a two dimensional body fitted grid containing 136 nodes in the flow wise direction and 24 nodes in the cross-wise direction. Low concentration levels for the eleven species calculated in the model allow the momentum and species conservation equations to be decoupled. This leads to a simplification of the solution methods for this problem which are pressure based.

The equation set modeled is provided below. The final model includes the numerical solution of 16 equations for the following 16 unknowns: x-velocity (u_1), y-velocity (u_2), pressure (p), turbulent kinetic energy dissipation rate (ε), turbulent kinetic energy (k) and 11 chemical species concentrations. The temperature variation within the reactor induced by radiant energy emitted by the TQ 718 lamp was not modeled at this time.

Mass Conservation:
$$\frac{\partial u_i}{\partial x_i} = 0 \tag{5}$$

Effective Viscosity:
$$\mu_{eff} = \mu + \mu_T = \mu + C_\mu \rho \frac{k^2}{\varepsilon} \tag{6}$$

RANS equation:
$$\rho \overline{u}_j \frac{\partial \overline{u}_i}{\partial x_j} = -\frac{\partial p \delta_{ij}}{\partial x_j} + \frac{\partial}{\partial x_j}(\mu_{eff}(\frac{\partial \overline{u}_i}{\partial x_j} + \frac{\partial \overline{u}_j}{\partial x_i})) \tag{7}$$

k-equation:
$$\rho \overline{u}_j \frac{\partial k}{\partial x_j} = \frac{\partial}{\partial x_j}((\mu + \frac{\mu_T}{\sigma k})\frac{\partial k}{\partial x_j}) - \rho\varepsilon + \mu_{eff} \frac{\partial \overline{u}_i}{\partial x_j}(\frac{\partial \overline{u}_i}{\partial x_j} + \frac{\partial \overline{u}_j}{\partial x_i}) \tag{8}$$

ε- equation:
$$\rho \overline{u}_j \frac{\partial \varepsilon}{\partial x_j} = \frac{\partial}{\partial x_j}((\mu + \frac{\mu_T}{\sigma_\varepsilon})\frac{\partial \varepsilon}{\partial x_j}) - \rho C_2 \frac{\varepsilon^2}{k} + C_1 \frac{\varepsilon}{k}\mu_{eff} \frac{\partial \overline{u}_i}{\partial x_j}(\frac{\partial \overline{u}_i}{\partial x_j} + \frac{\partial \overline{u}_j}{\partial x_i}) \tag{9}$$

RESULTS

The goal of the current modeling effort is to describe the physical and chemical processes occurring in a photolytic reactor and determine courses of action to increase the efficiency of the reactor in destroying HCHO. Parametric studies were performed which varied the inlet ozone concentration and the strength of the ultraviolet energy source. It was found that HCHO destruction by direct photolysis is an order of magnitude slower than by OH$^\bullet$ radical attack. For this reason methods were researched to increase the OH$^\bullet$ concentration in the reactor. The OH$^\bullet$ radical production can be enhanced by increasing the inlet ozone concentration and by increasing the strength of the ultraviolet energy source.

Effect of Ozone Inlet Concentration on HCHO Destruction

It was found, as was expected, that the destruction of HCHO increased with increasing O_3 inlet concentrations. This is due to the increased production of OH$^\bullet$ radicals from the reactions provided in Table 1. This is illustrated in Figure 2 which provides the HCHO concentration contours throughout the reactor for an inlet HCHO concentration of 1000 ppm and inlet ozone concentrations of 300 ppm and 75 ppm respectively. For the case where 75 ppm ozone is input into the system, the HCHO destruction is

ES96-47

confined in the bulb wake regions exclusively and is limited to 5% (50 ppm). The HCHO concentration with an inlet ozone concentration of 300 ppm, on the other hand, decreases to below 850 ppm, or 15% destruction in the immediate wake regions behind each bulb. This figure also illustrates that the region of HCHO destruction has been enhanced. HCHO destruction occurs over the top of the second bulb and well into the wake region behind the second bulb. The average destruction throughout the reactor for the high ozone condition is over 4% whereas an inlet ozone concentration of 75 ppm only resulted in an average 2% HCHO destruction in the reactor.

Although ozone enhances HCHO destruction, the model predicts that 90% of the ozone input into the reactor is discharged out the reactor outlet. This implies that an ozone scrubber might be required with a photolytic reactor design employing ozone to enhance VOC oxidation rates unless the ozone can be utilized in further oxidation processes in a given air pollution control system.

Effect of Light Intensity on HCHO Destruction

The light intensity emitted by the UV radiation source and the subsequent distribution of this radiation throughout the reactor has a significant impact on the overall destruction of HCHO in the reactor. The light intensity which is transmitted through the reactor, as shown by equation (1), depends on the concentration of chemical species in the reactor and on their respective absorption cross-sections. For this reason the light intensity distribution in the reactor will be different for different wavelengths of light. The light intensity distribution in the reactor at 254 nm (the wavelength of maximum ozone absorption) is provided in Figure 3. As shown in this figure, the light intensity drops off quickly with increasing distance from the UV light source. Less than 10% of the light is transmitted 2 bulb diameters downstream of the second bulb. This is an important discovery since the HCHO, O_3 and H_2O_2 photolysis reaction rates, and therefore HCHO destruction, are directly dependent on light intensity as shown in equation (2).

Based on Figure 3, it is therefore expected that the HCHO destruction will be significantly reduced as distance from the bulb surface is increased. This is illustrated in Figure 4 for the nominal light intensity case and for a 10-fold increase in light intensity. High rates of HCHO removal are illustrated in the wake regions behind the bulb surfaces but drop off significantly as distance from the bulb is increased in the flow wise direction. Figure 4 also shows, however, that a 10-fold increase in light intensity significantly enhanced HCHO destruction. The HCHO concentration drops to below 700 ppm, 30% HCHO destruction, in the wake regions with 10 fold increase in light intensity compared to 950 ppm, or 5% HCHO destruction for nominal light intensity. An average HCHO destruction rate across the outlet reactor is 14% for the 10-fold increase in light intensity compared to 1% for nominal light intensity conditions.

Interaction Between Gas Stream Advection and Chemical Reaction Rates on HCHO Destruction

Next the interaction between gas stream advection (hence residence time) and the chemical reaction rates was investigated. It was found that when the chemical reaction rates are much faster than the gas stream advection the species concentration distributions are unaffected by the flow field. An example is the OH$^{\bullet}$ concentration distribution in the reactor shown in Figure 5. The distribution essentially mimics the light intensity profile emitted by the TQ 718 lamps shown in Figure 3. HCHO (shown in Figure 2) and O_3 concentration distributions in the reactor, on the other hand, are influenced strongly by the reactor flow field. Figure 6 shows an overlay of the reactor velocity field on the HCHO concentrations contours. The concentration contours follow the velocity vectors which are overlaid on top. The acceleration of flow over the top surfaces of the bulbs result in lower destruction of HCHO whereas the recirculating regions behind the bulb surfaces lead to higher HCHO oxidation rates.

It is proposed that the recirculation regions in the bulb wake regions allow more contact time between the OH$^{\bullet}$ radicals and HCHO resulting in higher destruction efficiencies. Longer contact or

residence times in a given region are created by lower velocities in those regions. The HCHO destruction would therefore be expected to be high throughout the wake of the second bulb due to lower velocities in this region compared with velocities in the mainstream. This, however, does not occur because of the variable light intensity field modeled. When the light intensity was made uniform the HCHO destruction in the wake was enhanced to the edge of the reactor. There therefore exists an interaction between OH• distribution (related to light intensity distribution as show in Figures 3 and 5) and gas stream residence time that affects the spatial variability in HCHO destruction in the reactor.

The effects of residence time on HCHO removal were also investigated by varying the gas stream inlet velocity into the reactor. Inlet velocities were varied 0.5 m/s to 3.5 m/s. The highest HCHO removal occurred for the lowest inlet velocity case with negligible destruction occurring for an inlet velocity of 3.5 m/s. For an inlet ozone of 300 ppm, an inlet velocity of 0.5 m/s resulted in an average HCHO destruction of over 4% whereas an inlet velocity of 3.5 m/s resulted in an average HCHO destruction of less than 1%.

CONCLUSIONS

Based on the results of this modeling study, a photolytic reactor design should have close placement and arrangement of UV bulbs (one to two bulb diameters) to optimize light intensity distribution. The UV lamps should also be chosen to maximize power output in the wavelength ranges that produce photolysis of the target VOC and ozone. If the bulbs are placed too far apart, part of the gas stream will remain essentially untreated due to the decrease of light intensity (hence OH• radical concentration) with distance from the bulb. A photolytic reactor design should also optimize recirculation of the process gas stream within the reactor to increase gas stream residence time near the bulb surfaces.

REFERENCES

Albano, M.; *Computer Simulation of a Photolytic Reactor to Study the Effects of a Variety of Wavelengths*. A Thesis in Environmental Pollution Control, The Pennsylvania State University, State College, Pa., 1994.

Anatasi, C., Gladstone, R. V., Sanderson, M. G.; Environmental Sci. Technol. **1993** 27(3): 474-482.

Atkinson, R., Baulch, D. L., Cox, R. A., Hampson, R. F., Kerr, J. A., Troe, J., J. Phys. Chem. Ref. Data **1992** 21:1125-1173.

Calvert, J. G., Pitts, J. N.; *Photochemistry*; John Wiley & Sons, New York, 1966.

DeMore, W. B., Sander, S. P., Golden, D. M., Hampson, R.F., Kurylo, M. J., Howard, C. J., Ravishankara, A. R., Kolb, C. E., Molina, M. J.; *Chemical Kinetics and Photochemical Data for Use in Stratospheric Modeling*, JPL Publication 92-20, 1992.

Mallery, M.; *Numerical Model of Formaldehyde Photo-oxidation in a Two-Dimensional Flow Field Over Cylindrical UV Light Sources*. A Thesis in Mechanical Engineering, The Pennsylvania State University, State College, Pa., 1995.

Schmelzle, J. P.;*Ultraviolet Photochemical and Radical Oxidation of Airborne Volatile Organic Compounds*. A Thesis in Environmental Pollution Control, The Pennsylvania State University, State College, Pa., 1994.

NOMENCLATURE

C	Species Concentration	r	Distance from bulb	ϕ	Quantum Yield
D	Molecular Diffusion Coefficient	r_o	Bulb radius	ρ	Gas Density
I_{ro}	Light Intensity bulb Surface	U	Gas Velocity	σ	Absorp. Cross-Sect.
$J(\lambda)$	Actinic Flux	μ_T	Turbulent Viscosity	σ_S	Turbulent Prandtl No.

Table 1 Chemical reactions incorporated into flow field model of reactor.

Radical Oxidation Reactions Modeled

Chemical Reaction	Rate Constant (cm^3/molecule)	Reference
$OH^\bullet + O_3 \rightarrow HO_2^\bullet + O_2$	6.8e-14	DeMore *et al.*, 1992
$HO_2^\bullet + O_3 \rightarrow OH^\bullet + 2O_2$	2.0e-15	DeMore *et al.*, 1992
$HCO^\bullet + O_2 \rightarrow HO_2^\bullet + CO$	5.5e-12	DeMore *et al.*, 1992
$OH^\bullet + OH^\bullet \rightarrow O(^1D) + H_2O$	1.9e-12	DeMore *et al.*, 1992
$OH^\bullet + HO_2^\bullet \rightarrow O_2 + H_2O$	1.1e-10	DeMore *et al.*, 1992
$OH^\bullet + H_2O_2 \rightarrow HO_2 + H_2O$	1.7e-12	DeMore *et al.*, 1992
$CO + OH^\bullet \rightarrow CO_2 + H^\bullet$	1.5e-12	DeMore *et al.*, 1992
$HCHO + OH^\bullet \rightarrow HCO^\bullet + H_2O$	1.0e-11	DeMore *et al.*, 1992
$H^\bullet + O_2 \xrightarrow{M} HO_2$	1.2e-12	Anastasi *et al.*, 1993
$H^\bullet + O_3 \rightarrow OH + O_2$	2.9e-11	DeMore *et al.*, 1992
$HO_2^\bullet + HO_2^\bullet \rightarrow H_2O_2 + O_2$	1.6e-12	DeMore *et al.*, 1992
$CO + HO_2^\bullet \rightarrow CO_2 + OH^\bullet$	1.9e-32	DeMore *et al.*, 1992
$O(^1D) + N_2 \rightarrow O(^3P) + N_2$	2.6e-11	DeMore *et al.*, 1992
$O(^3P) + O_2 \xrightarrow{M} O_3$	1.0e-14	DeMore *et al.*, 1992
$O(^1D) + H_2O \rightarrow OH^\bullet + OH^\bullet$	2.2e-10	DeMore *et al.*, 1992
$O(^1D) + O_2 \rightarrow O(^3P) + O_2$	4.0e-11	DeMore *et al.*, 1992
$CH_3OH + OH^\bullet \rightarrow CH_2OH + H_2O$	7.8e-13	Atkinson *et al.*, 1992
$CH_3OH + OH^\bullet \rightarrow CH_3O + H_2O$	1.4e-13	Atkinson *et al.*, 1992

Photolytic Reactions Modeled

Chemical Reaction	Rate Constant at the Bulb Surface (seconds^{-1})	Reference
$HCHO + hv \rightarrow H^\bullet + HCO^\bullet$	0.0091	Calvert *et al.*, 1966
$HCHO + hv \rightarrow H_2 + CO$	0.0033	Calvert *et al.*, 1966
$O_3 + hv \rightarrow O_2 + O(^1D)^\bullet$	1.900	Atkinson *et al.*, 1992
$O_3 + hv \rightarrow O_2 + O(^3P)^\bullet$	0.2150	Atkinson *et al.*, 1992
$H_2O_2 + hv \rightarrow OH^\bullet + OH^\bullet$	0.0133	Atkinson *et al.*, 1992

Process
Gas
Stream

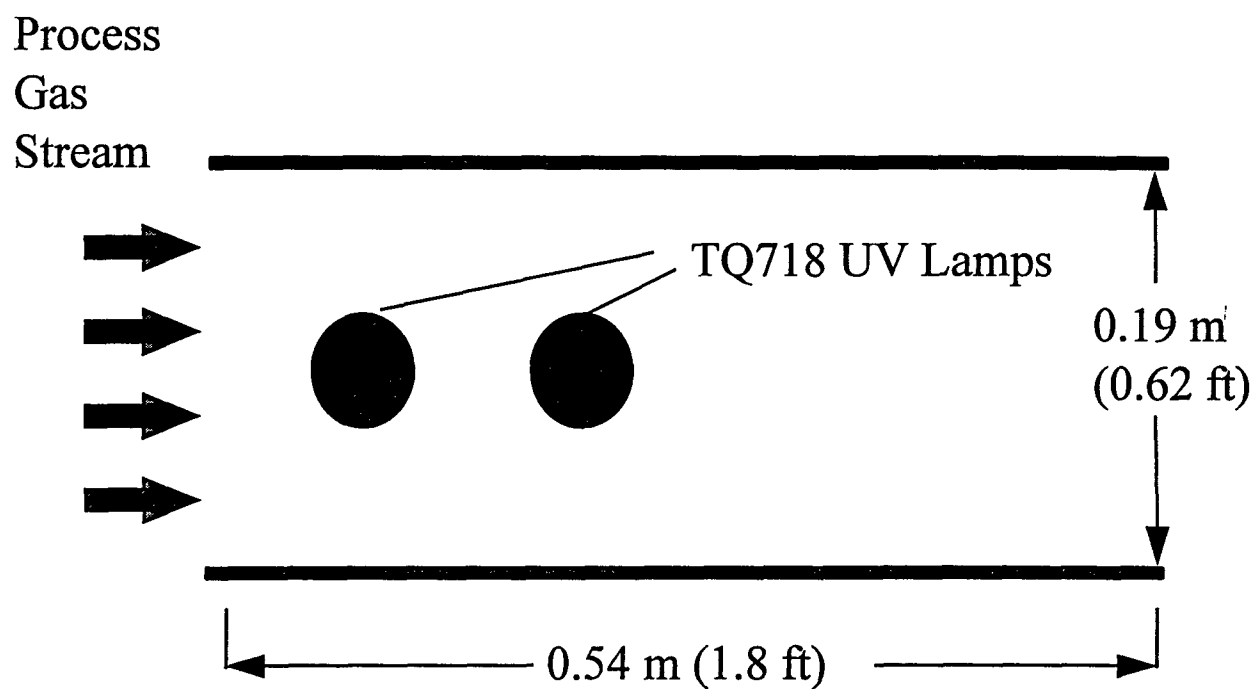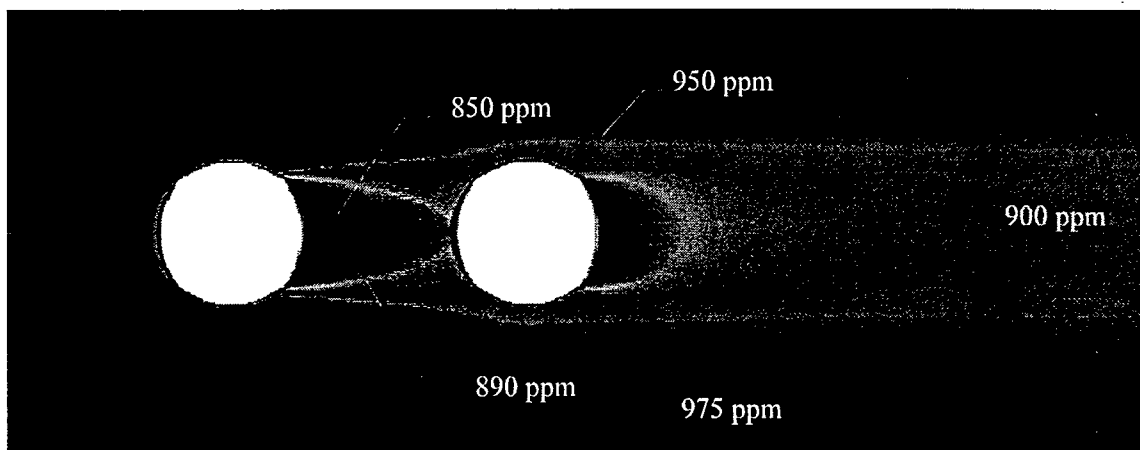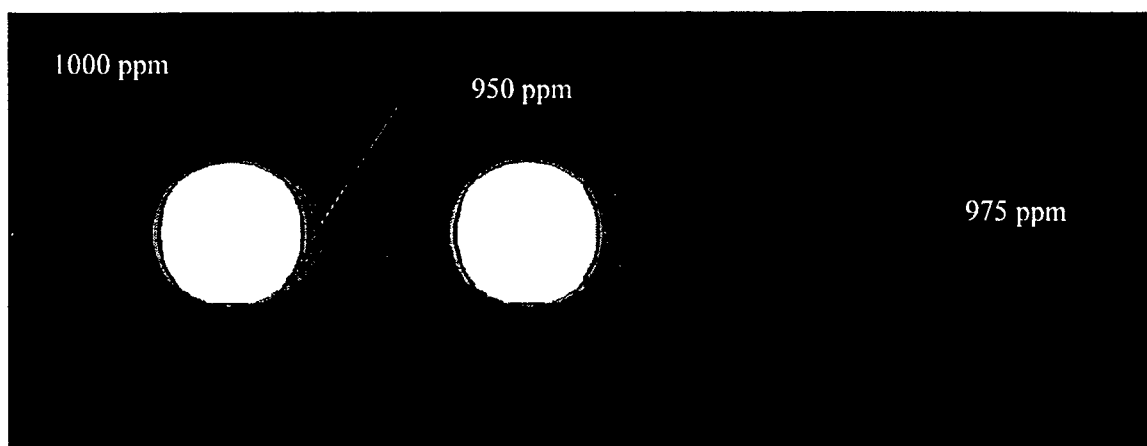TQ718 UV Lamps

0.19 m
(0.62 ft)

0.54 m (1.8 ft)

Figure 1 Photolytic reactor

Ozone Inlet Concentration of 300 ppm, Air Stream Inlet Velocity of 0.5 m/s

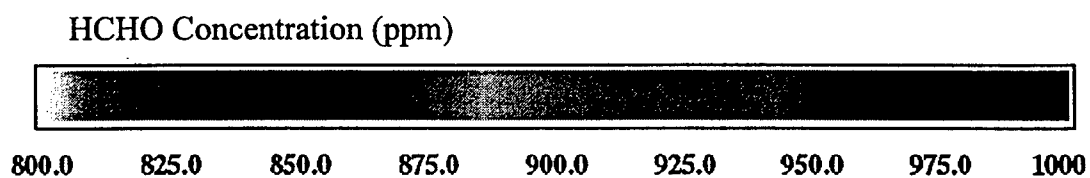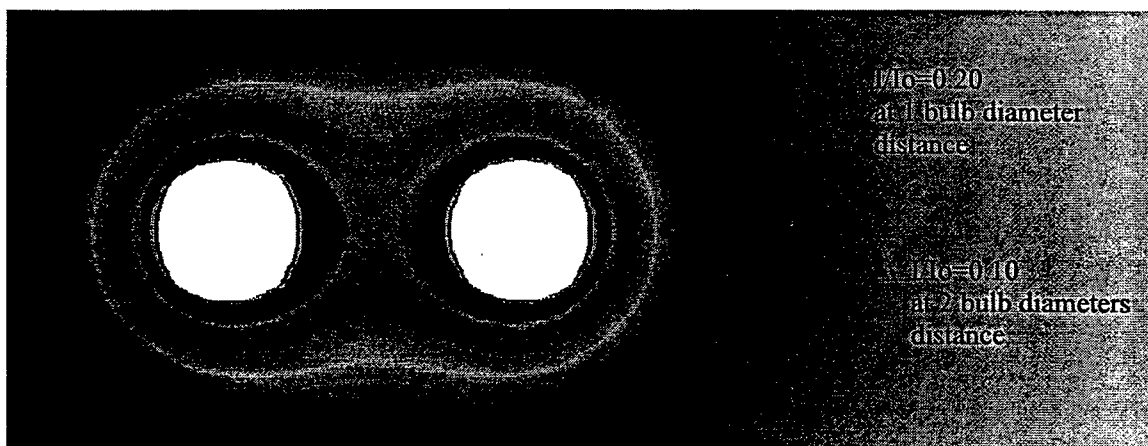Ozone Inlet Concentration of 75 ppm, Air Stream Inlet Velocity 0.5 m/s

HCHO Concentration (ppm)

| 800.0 | 825.0 | 850.0 | 875.0 | 900.0 | 925.0 | 950.0 | 975.0 | 1000 |

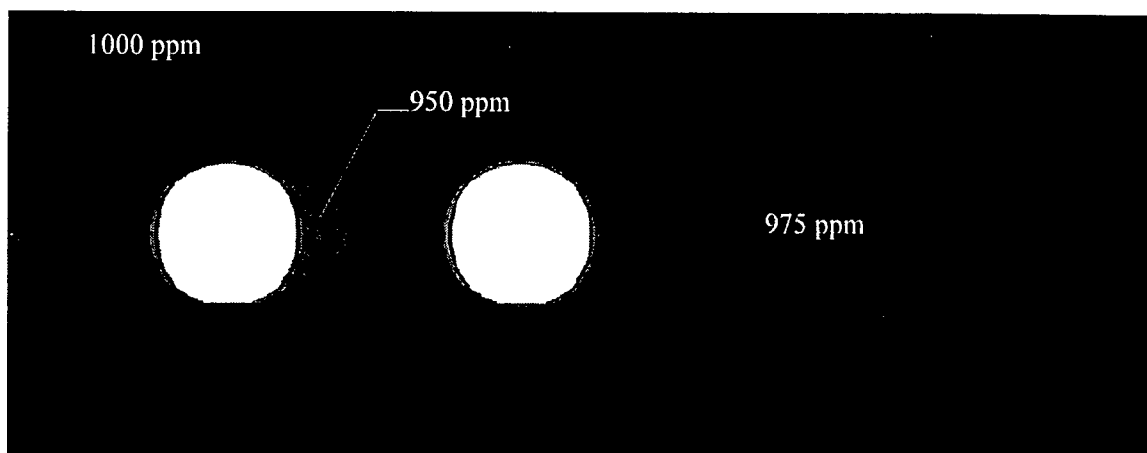Figure 2 Effect of inlet ozone concentration on HCHO removal in the reactor.

I/Io=0.20
at 1 bulb diameter
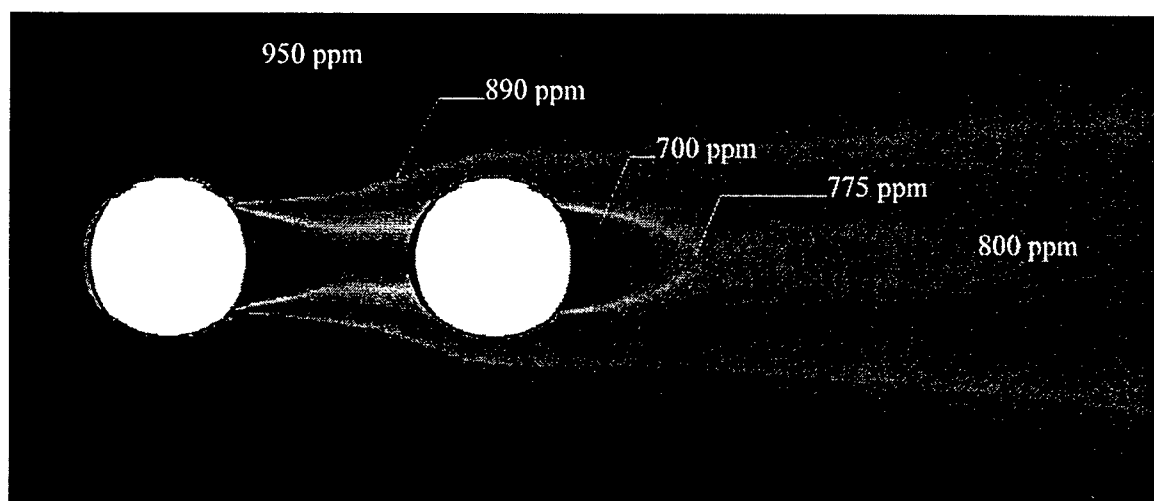distance

I/Io=0.10
at 2 bulb diameters
distance

Light Intensity I/Io

| 0.0 | 0.1 | 0.2 | 0.3 | 0.4 | 0.5 | 0.6 | 0.7 | 0.8 | 0.9 | 1.0 | 1.: |
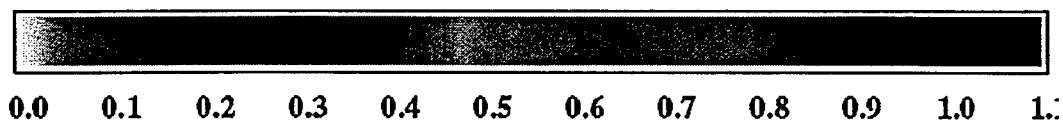
Figure 3 Light intensity distribution in the reactor at 254 nm

Nominal Light Intensity, Air Stream Inlet Velocity 2 m/s

1000 ppm

950 ppm

975 ppm

10 Fold Increase in Light Intensity, Air Stream Inlet Velocity 2 m/s

950 ppm

890 ppm

700 ppm

775 ppm

800 ppm

HCHO Concentration (ppm)

600.0   650.0   700.0   750.0   800.0   850.0   900.0   950.0   1000
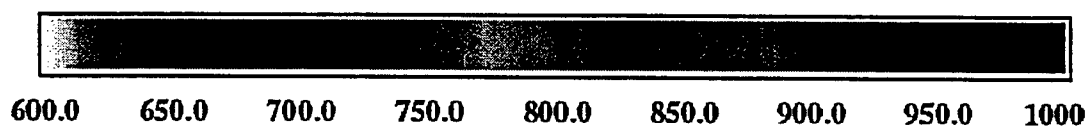
Figure 4 Effect of light intensity on HCHO destruction in the reactor.

OH Concentration (ppm)

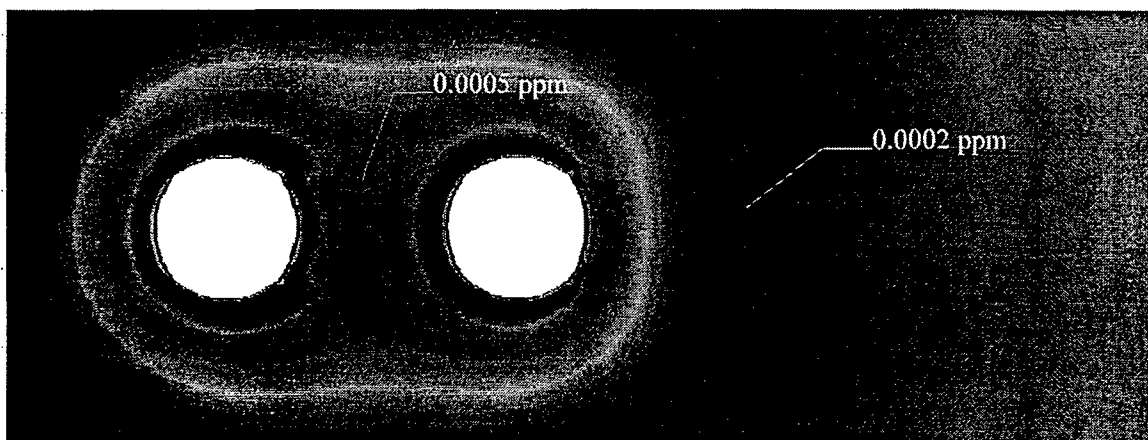0.0000 0.0001 0.0002 0.0003 0.0004 0.0005 0.0006 0.0007 0.0008 0.000
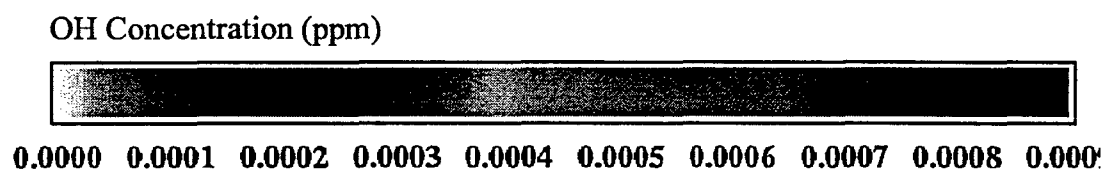
Figure 5 OH concentration distribution in the reactor for an inlet velocity of
0.5 m/s and an ozone concentration of 300 ppm.

HCHO Concentration (ppm)

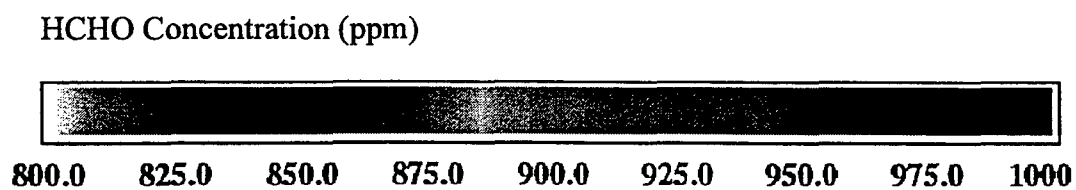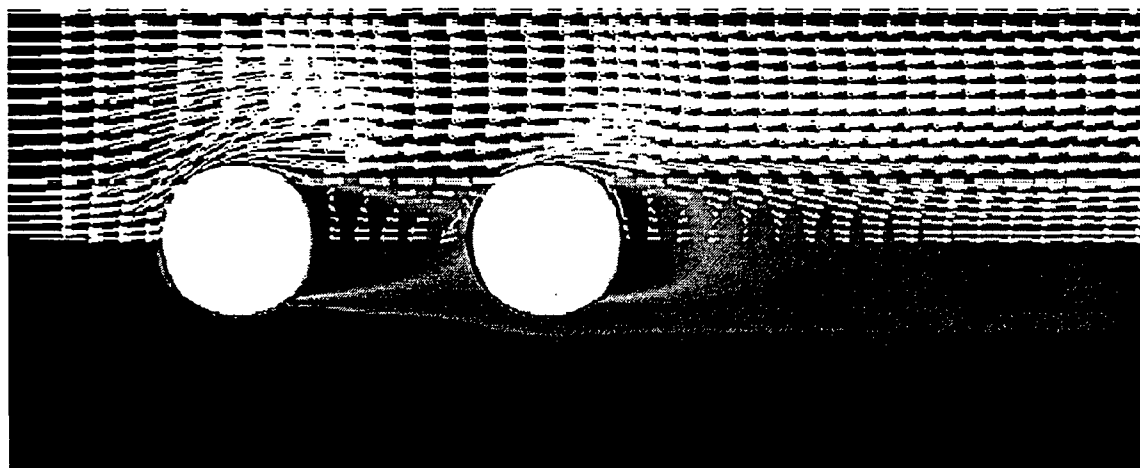800.0   825.0   850.0   875.0   900.0   925.0   950.0   975.0   1000

Figure 6 Velocity vector plot and HCHO concentration contours for an inlet
velocity of 0.5 m/s and an inlet ozone concentration of 300 ppm.